Prediction error filters to enhance differences

Robert G. Clapp[1]

ABSTRACT

Prediction Error Filters (PEFs) capture the covariance of a dataset. In this paper I use PEFs to quantify and highlight difference between two volumes. A series of PEFs are estimated on one volume and then applied to a second. The resulting hypercube is an indicator of where, and how much, two volumes differ.

INTRODUCTION

Developing and debugging a new approach to an old problem involves constantly comparing your 'improved' result to the 'old' approach. For 2-D volumes a movie flipping between the 'old' and 'improved' images is an effective mechanism for the well trained eye. When the dimensionality of your volume increases and/or the training of the observer decreases the human eye approach becomes less useful.

Prediction Error Filters (PEFs) (Claerbout, 1999) provide an estimate of a volume's inverse covariance, with *stationary* statistics. By using non-stationary Prediction Error Filters (Crawley et al., 1998) or by breaking the problem into patches (Claerbout, 1992) we can characterize some level of non-stationary statistics. Schwab (1998) showed that by estimating a PEF within small patches and then applying the filter on the patch, event's subtle features such as faults become more visible.

In this paper I use a variation on the same technique to highlight differences between volumes ('a' and 'b'). I estimates PEFs within small patches on one volume 'a' then apply the PEF to both 'a' and 'b'. I then apply a simple algebraic combination of the volumes resulting from applying the PEF to form a measure of image difference. I compare this technique to a more standard histogram matching approach and apply it on both 2-D and 3-D volumes.

METHODOLOGY

PEFs attempt to capture the inverse spectrum of the data. In the 1-D case, we could calculate a filter with the inverse spectrum by transforming into the frequency domain and then doing a sample by sample division,

[1]**e-mail:** bob@sep.stanford.edu,

$$Y(\omega) = \frac{1}{D(\omega)}, \tag{1}$$

where $Y(\omega)$ is the filter and $D(\omega)$ is the data in the Fourier domain. There are two problems with this approach. First $D(\omega)$ can be small or zero valued and $y(t)$ is not compact. Claerbout (1999) shows that a compact filter can be estimated by solving the least squares system

$$\mathbf{y} = (\mathbf{D}'\mathbf{D})^{-1}\mathbf{D0}, \tag{2}$$

where $\mathbf{y}$ is a filter whose zero lag is fixed at one, $\mathbf{0}$ is a vector of 0s, and $\mathbf{D}$ is convolution with the data. In general the shape of filter is arbitrary but needs to be large enough to capture the spectrum of the wavelet and the dips present in the volume.

The residual $\mathbf{r}$ of the estimation procedure can be calculated by convolving the filter $\mathbf{Y}$ with the data

$$\mathbf{r} = \mathbf{Yd}. \tag{3}$$

The residual will be large when the filter is not large enough to fully describe the stationary spectrum or the data is non-stationary. The left panel of Figure 1 shows the result of migrating the Marmousi dataset using a standard downward continuation based migration. The right panel shows the result of first estimating a series of PEFs in overlapping patches on the migrated image and then applying the PEFs to the migrated volume (applying equation 3). Note the areas of large residual generally correspond to unconformities and fault locations.

The next step is to apply this same series of PEFs to another image. The first question is what happens if we apply a filter estimated on volume 'a' to volume 'b' which has significantly different spatial statistics. The left panel of Figure 2 shows a simple plane wave. The right panel of Figure 2 shows the result applying the filters estimated from the Marmousi migration. The dominant feature is still the planewave. The amplitude of the residual is on average an order of magnitude higher than the residual shown in the right panel of Figure 1. If dataset 'b' has a spectrum close to 'a' we get a different result. We should see large values at both where the stationarity assumption of the PEF is invalid and at places where the covariance description of 'a' and 'b' are different. Figure 3 illustrates this point. Both the left panel of Figure 1 and 3 are calculated by a source-receiver Phase-Shift Plus Interpolation (PSPI) algorithm. The left panel of Figure 1 shows the result of using up to eight reference velocities, the left of panel of Figure 3 uses a single reference velocity at each depth step. The right panel of Figure 3 shows the result of applying equation3 using the filter calculated from the eight velocity migration. Note that in addition to the large residual locations seen in the right panel of Figure 1, we now see additional locations. Generally the large values are at and below areas of large dip, where the first order split step correction is least accurate.

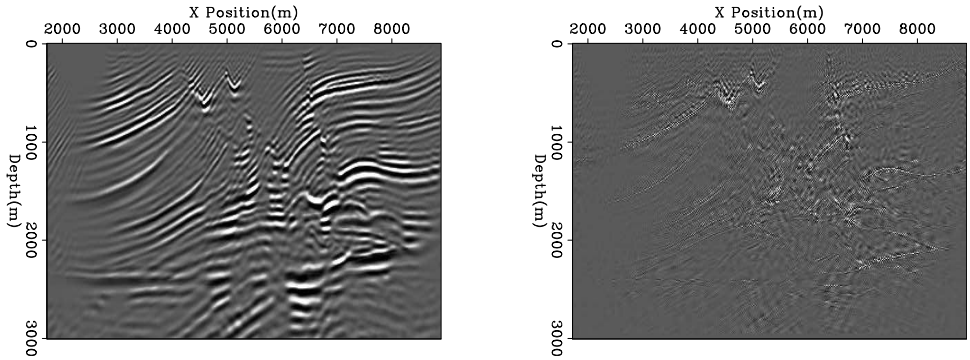

Figure 1: The left panel the result of PSPI migration of the Marmousi dataset using 8 reference velocities. The right panel shows the result of equation 3.

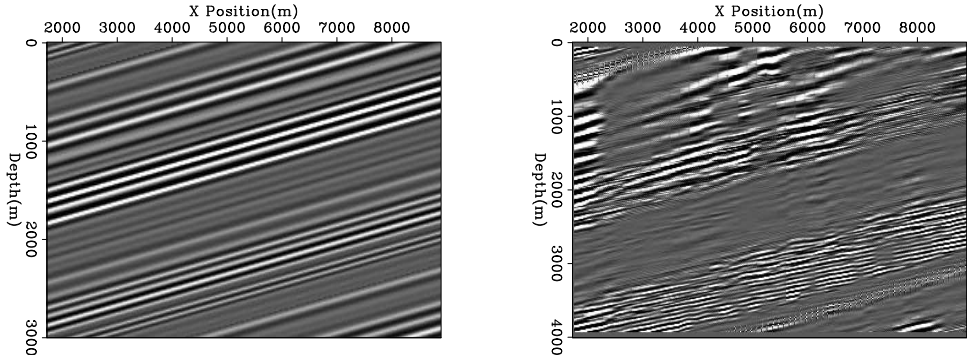

Figure 2: The left panel is a planewave. The right panel is the result of applying the filter estimated from the 8 velocity Marmousi image.

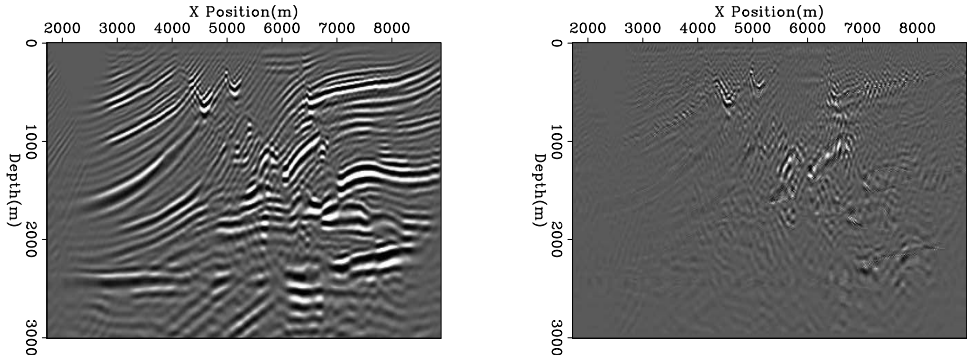

Figure 3: The left panel is the result of PSPI migration of the Marmousi dataset using one reference velocity. The right panel shows the result of equation 3 using filters calculated from the data shown in the left panel of Figure 1.

What we really would like is just the differences caused by the change in the migration algorithm. For notational convenience we will define $\mathbf{r_{a,b}}$ as the residual of applying a filter estimated on dataset 'a' to dataset 'b'. Simply dividing $\mathbf{r_{a,a}}$ by $\mathbf{r_{a,a}}$ is not feasible due to the zero in $\mathbf{r_{a,a}}$. One approach to this problem is adding an epsilon term to the denominator. Another approach is smoothing. We first take the absolute value $\mathbf{A}$, and then smooth the resulting volume. As a result, we end up with an estimate of the fitting error $\mathbf{e}$,

$$\mathbf{e} = \frac{\mathbf{SAr_{a,b}}}{\mathbf{SAr_{a,a}}} - \mathbf{1} \tag{4}$$

An alternate approach is to add a scaling term that emphasizes errors where the original data is large. We can do this by applying a smoothed envelope function $\mathbf{E}$ to dataset $\mathbf{a}$,

$$\mathbf{e}_{\text{scaled}} = \mathbf{Ea}\left(\frac{\mathbf{SAr_{a,b}}}{\mathbf{SAr_{a,a}}} - \mathbf{1}\right). \tag{5}$$

Figure 4 shows the result of applying equation 5 comparing the one and eight reference velocity images. Note how the differences are located at steep dips, where we would anticipate the single reference velocity approach failing.

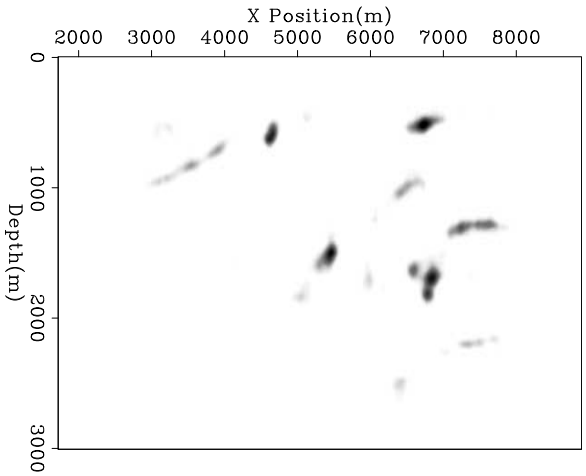

Figure 4: The result of applying equation 5 comparing the one and eight reference velocity images.

HISTOGRAM NORMALIZATION

The previous section discussed a covariance-based approach to compare two volumes. In this section I will discuss a more tradition amplitude-based approach. Strict differences between the volumes is an option in some instances but often approaches have significantly different amplitude profiles. One solution is called histogram equalization.

My implementation of this approach is to first calculate the amplitude in volume 'a' at several different quantiles

$$m_a(i) = Q(a, i), \tag{6}$$

where m_a is the amplitude at a given percentile i of volume a using the quantile function Q. The vector m_a is basically a discrete version of the data's cumulative distribution function (CDF). I then found the amplitude in volume 'b' at the same quantiles producing the amplitude map m_b. Figure 5 shows the cumulative distribution function for the one and eight velocity PSPI migrations shown in the previous section. Note how the two curves are similar, diverging only at their edges. Finally I looped through volume 'b', for each sample I found its approximate quantile by finding the samples of m_b that contained the value and performing linear interpolation. I was able to remap into the amplitude profile of 'a' using m_a. Figure 6 shows the difference between the one and eight reference velocity PSPI migration after histogram normalization. Note the image seems to emphasize the major reflectors of the image rather than the differences.

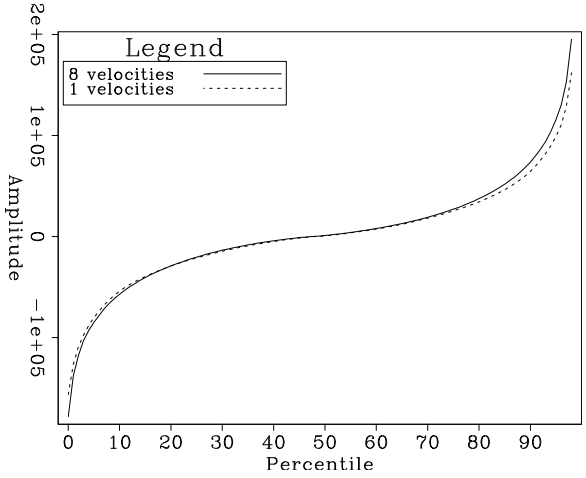

Figure 5: The solid curve is the CDF for the eight velocity PSPI migration shown in Figure 1, the dashed curve shows the CDF using one velocity (shown in Figure 3). Note how the two curves are similar diverging only at their edges.

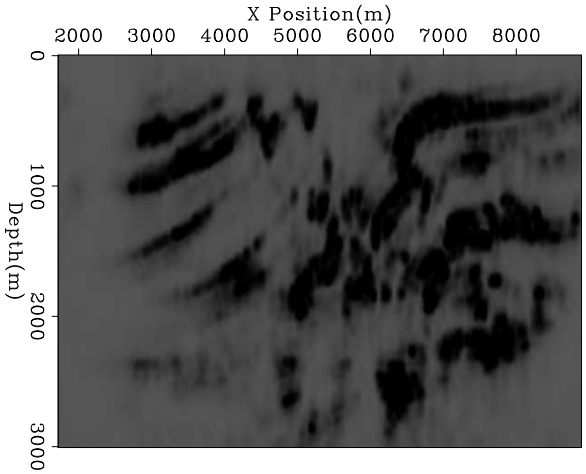

Figure 6: The difference between the one and eight reference velocity PSPI migration after histogram normalization.

PRECISION

Fu et al. (2007) implements some of the core algorithms in reverse time migration and downward continuation based migration on a FPGA. In many situations compute

speed can be traded for precision on a FPGA. Clapp (2007) showed that migration is well suited for reduced precision given the summation implied by the process.

Fu et al. (2007) uses a non-linear, computer driven scheme to test whether a given number representation effects the computed result. In order to use this scheme, some test of whether a result changed in a meaningful way had to be designed. The methodology discussed above offers that potential. By summing up the errors resulting from applying equation 5 a single number that represents how well the covariance of an image has been preserved can obtained.

To test this methodology I applied the same precision limiting scheme described in Clapp (2007).The rows of Figure 7 shows the result of limiting the precision of the FK, FFT, and FX portions of the downward continuation process to 3,5, and 9 bits. The left panel is the zero subsurface offset image in each case. The center panel the error calculation using the PEF method. The right panel shows the result using the histogram matching scheme. In each case the migration result is compared against the full precision image. Note how the errors drastically decreases between 3 and 5 bits. Figure 8 show the total error for 3-9 bits. In this case, both methods seem to be an effective mechanism for testing accuracy. Note how the curve dramatically decreases between 3 and 6 bits then remains relatively constant for the PEF method scheme. The elbow in each curve curve represents the best tradeoff between bit precision and accuracy.

REFERENCE VELOCITIES

The bit precision limiting scheme used in the previous section should either have a relatively uniform, or somewhat unpredictable, amplitude effect. A more interesting test is to apply both difference detecting methodologies on a problem where the locations of the differences are well known.

PSPI migration accurately handles non-overturning waves when the velocity in a given depth layer is constant. When velocity varies laterally the accuracy decreases as a function of propagation angle. The Marmousi example has significant lateral velocity variation and many steeply dipping events. As a result the image quality varies with the number of reference velocities that are used. Figure 9 shows the effect of changing the number of reference velocities used in the migration.The rows represent migrating with a PSPI migration using one, three, and seven reference velocities. The left column is the migrated image, the center panel is the result of using the PEF method for detecting differences. The right panel shows the result of using the histogram matching. In this case, the PEF approach proves to be better at identifying differences in the images. Note how the PEF approach highlights the steeply dipping features, where the PSPI approximation breaks down. With increasing number of reference velocities only steeper dipping features are displayed. The histogram approach seems to simply highlight the major features in the image, showing limited preference towards large dips. Figure 10 shows the total differences

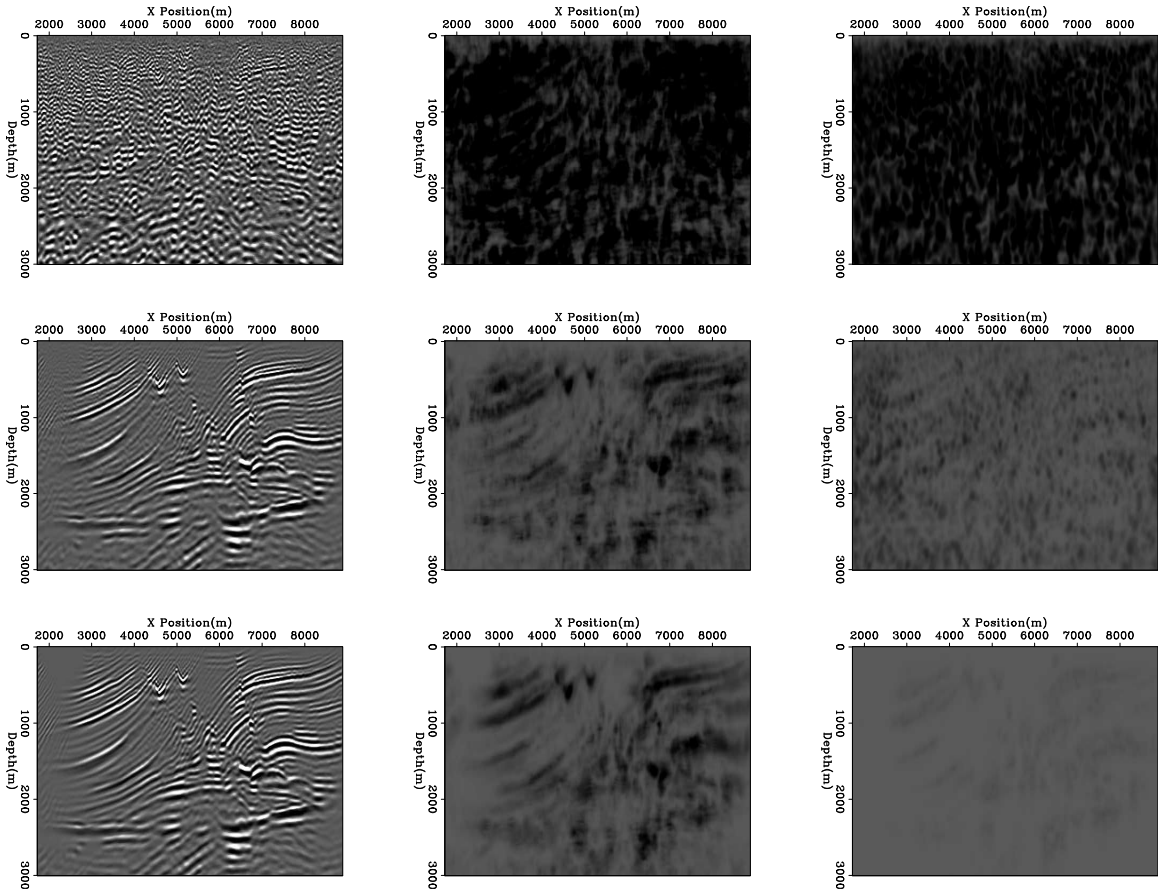

Figure 7: The shows the result of limiting the precision of the FK and FX portions of the downward continuation process to 2,4, and 9 bits. The left panel is the zero subsurface offset image in each case. The center (PEF) and right (histogram based) panel are the error calculation. In each case the migration result is compared; against the full precision image.

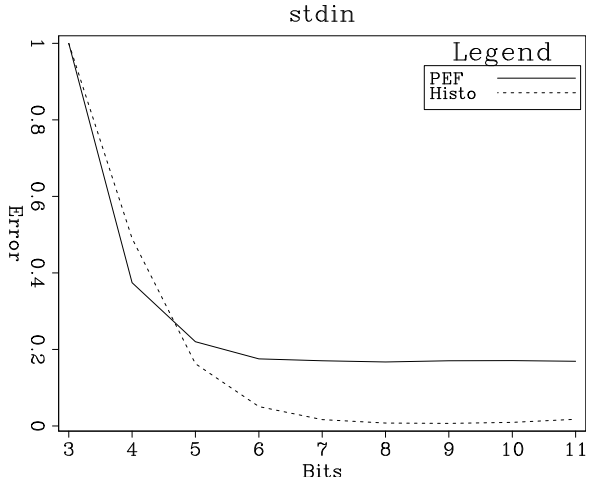

Figure 8: Error vs. bit representation for PSPI migration. Note the elbow in the curve represents the best tradeoff between bit precision and accuracy.

as a function of the number of reference velocities. Note how the effect of increasing the number of reference velocities is much more pronounced in the PEF case.

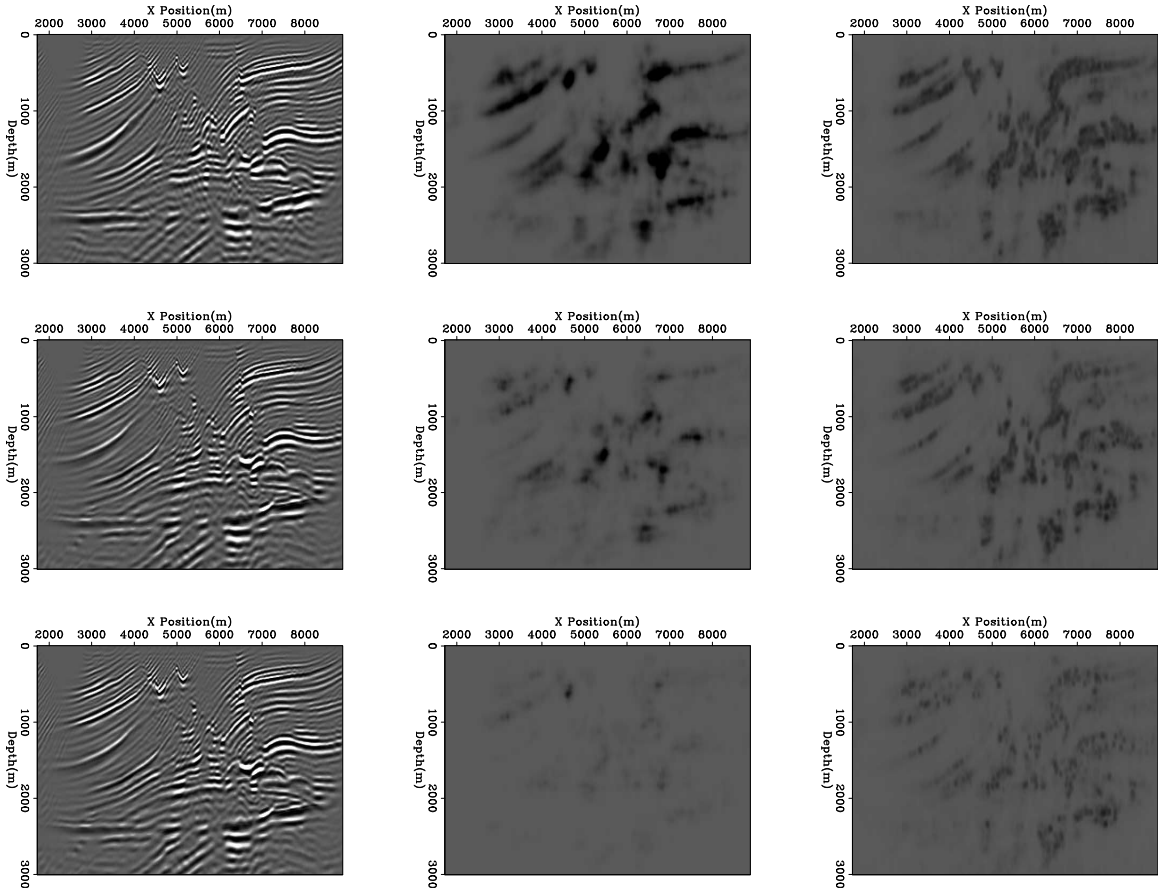

Figure 9: The rows represent migrating with a PSPI migration using one, three, and seven reference velocities. The left column is the migrated image, the center panel is the result of using the PEF method for detecting differences. The right panel shows the result of using the histogram matching.

PLANEWAVE MIGRATION

As demonstrated in the last section the PEF method has the ability to highlight subtle differences in images. In this section, I apply the methodology to 3-D planewave migrated cubes. The first uses a conventional scheme, the second uses the tilted-coordinate approach described in Shan and Biondi (2007). I broke the image into 30x30x30 patches and used a 3-D PEF that was 8x3x3 in size.

Figure 11 shows three orthogonal slices through a volume migrated with a conventional planewave migration algorithm. Note the salt structure top is poorly delineated in the inline section. Figure 12 shows the same three orthogonal slices using a tilted planewave migration scheme. Note how salt top is significantly better delineated.

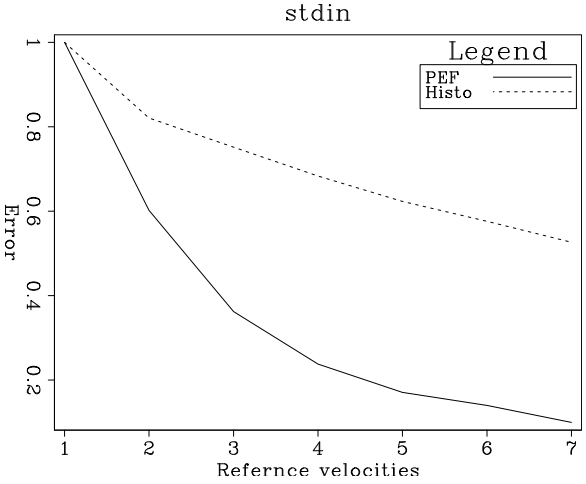

Figure 10: A graph of the differences detected by the PEF (solid line) and histogram matching (dashed line) scheme.

Figure 13 shows the result of apply the PEF scheme compared the two 3-D migrated cubes. In the depth slice, the salt structure is highlighted. In addition, several faults become evident. The inline panel and crossline panel highlight the salt top. A subtle fault feature is visible in the crossline and a high-spatial frequency even is evident in the inline. Figure 14 shows the result of using the histogram methodology. The method proves generally ineffective in highlighting any differences other than the salt top.

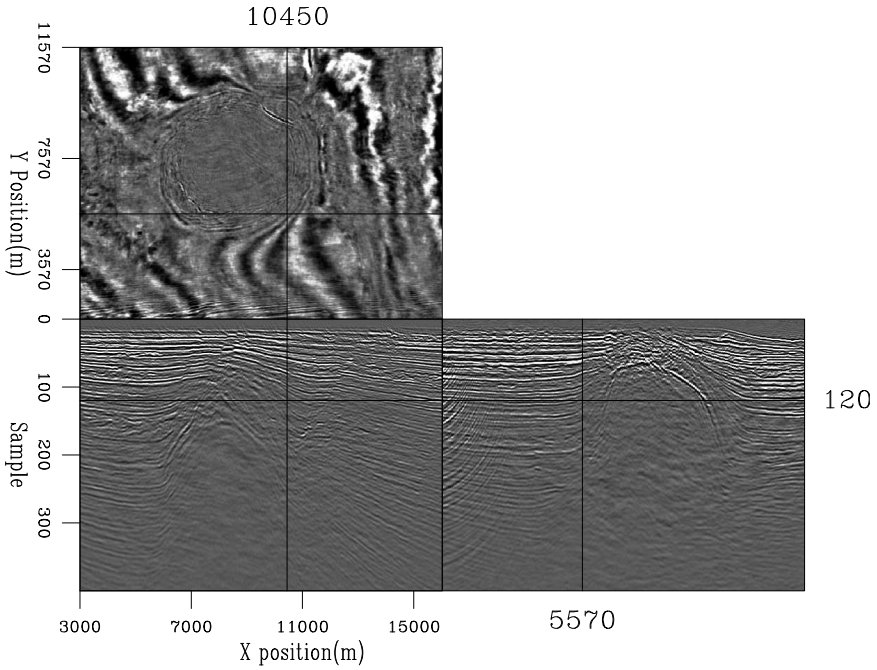

Figure 11: Three orthogonal slices through a migrated cube using a conventional planewave migration algorithm.

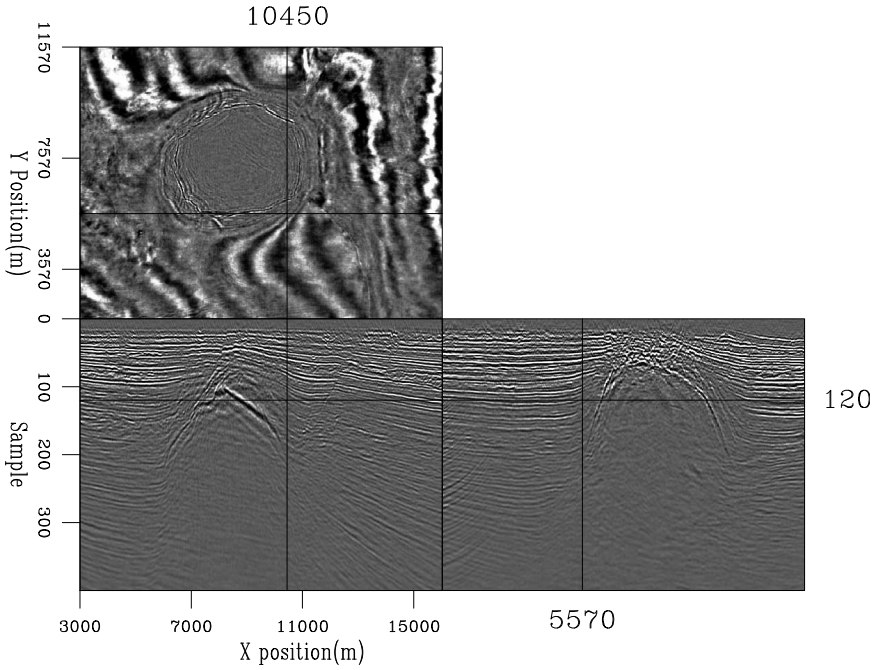

Figure 12: The same slices seen in Figure 11, now through a volume migrated with a tilted-coordinate planewave migration algorithm.

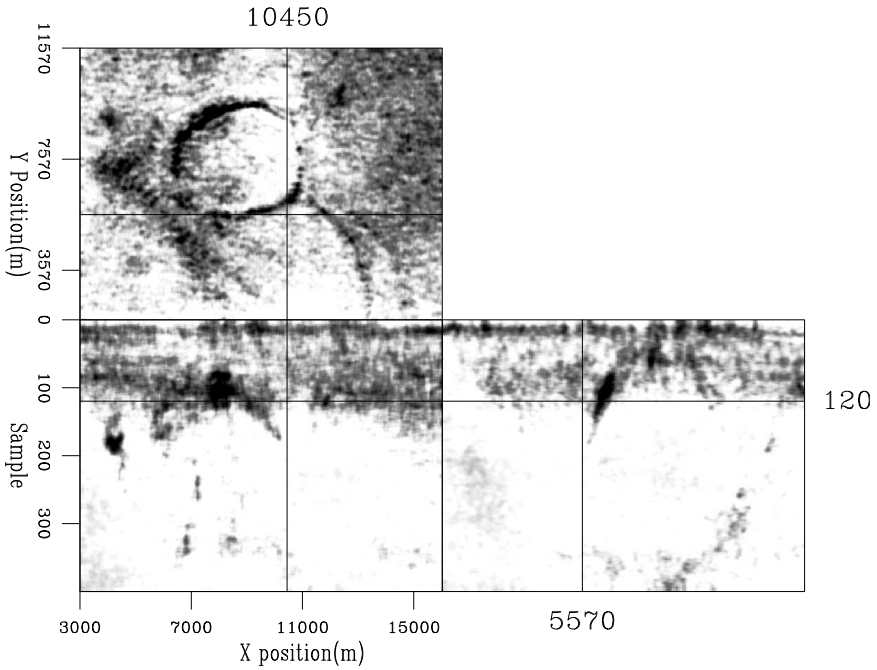

Figure 13: The same slices seen in Figure 11- 12 through a volume created by applying equation 5 to the volumes shown in the previous two figures. Note the highlighting of the salt reflection along with several faults.

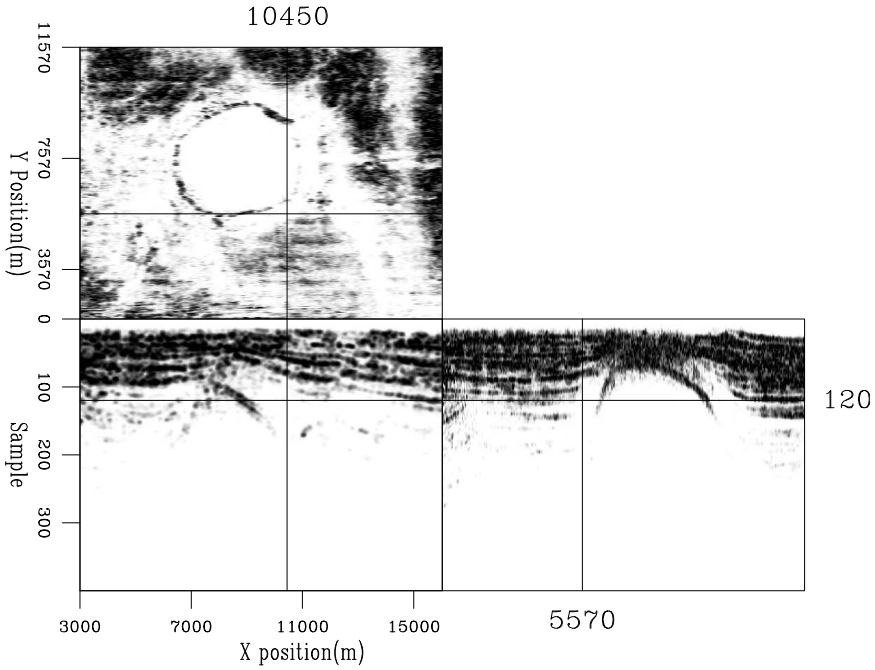

Figure 14: The same slices seen in Figure 11- 13 through a volume created by applying the histogram matching approach. Note how the salt top is visible but the fault features seen Figure 14 are not.

CONCLUSIONS

Two schemes, one amplitude based, one covariance based, are described that automatically compare two seismic images. The first scheme uses histogram normalization to equalize the amplitude of the full precision and reduced precission volumes. The second approach compares the covariance of two volumes within small patches. Both methods prove effective, with the covariance based approach showing more consistent behavior.

ACKNOWLEDGMENTS

I would like to thank ExxonMobil for the dataset. I would like to acknowledge Oskar Mencer who insisted that I do this work. Biondo Biondi suggested that histogram normalization would be worth trying.

REFERENCES

Claerbout, J., 1999, Geophysical estimation by example: Environmental soundings image enhancement: Stanford Exploration Project.

Claerbout, J. F., 1992, Nonstationarity and conjugacy: Utilities for data patch work: SEP-Report, **73**, 391–400.

Clapp, R. G., 2007, Moveout analysis with flattening: SEP-Report, **129**, 149–158.

Crawley, S., R. Clapp, and J. Claerbout, 1998, Decon and interpolation with nonstationary filters: SEP-Report, **97**, 183–192.

Fu, H., W. Osbourne, R. G. Clapp, and O. Mencer, 2007, Accelerating seismic computations using customized number representations on fpgas: SEP-Report, **131**.

Schwab, M., 1998, Enhancement of discontinuities in seismic 3-D images using a Java estimation library: PhD thesis, Stanford University.

Shan, G. and B. Biondi, 2007, Angle domain common image gathers for steep reflectors: SEP-Report, **131**.